

Arbuscular cell invasion coincides with extracellular vesicles and membrane tubules

Ronelle Roth¹, Stefan Hillmer², Charlotta Funaya², Marco Chiapello³, Karin Schumacher⁴, Libera Lo Presti^{5,6}, Regine Kahmann⁵ and Uta Paszkowski^{1*}

During establishment of arbuscular mycorrhizal symbioses, fungal hyphae invade root cells producing transient tree-like structures, the arbuscules, where exchange of photosynthates for soil minerals occurs. Arbuscule formation and collapse lead to rapid production and degradation of plant and fungal membranes, their spatiotemporal dynamics directly influencing nutrient exchange. We determined the ultra-structural details of both membrane surfaces and the interstitial apoplastic matrix by transmission electron microscopy tomography during growth and senescence of *Rhizophagus irregularis* arbuscules in rice. Invasive growth of arbuscular hyphae was associated with abundant fungal membrane tubules (memtubs) and plant peri-arbuscular membrane evaginations. Similarly, the phylogenetically distant arbuscular mycorrhizal fungus, *Gigaspora rosea*, and the fungal maize pathogen, *Ustilago maydis*, developed memtubs while invading host cells, revealing structural commonalities independent of the mutualistic or parasitic outcome of the interaction. Additionally, extracellular vesicles formed continuously in the peri-arbuscular interface from arbuscule biogenesis to senescence, suggesting an involvement in inter-organismic signal and nutrient exchange throughout the arbuscule lifespan.

Arbuscular mycorrhizal symbiosis is an ancient symbiosis between the roots of most plant species and fungi of the Glomeromycotina that evolved concurrently with land plants around 450 million years ago and, ever since, has represented an integral part of plant terrestrial ecosystems (for a recent review, see ref. ¹). The outcome of the symbiosis is mutualistic, manifested in a bi-directional transfer of soil minerals such as inorganic phosphate in exchange for host-derived carbon. Central to this symbiotic nutrient exchange are specialized fungal feeding structures called arbuscules, that form within root cortical cells. Arbuscular development starts with the establishment of a ‘trunk’ domain from which sequential dichotomous hyphal branching and tip growth produce coarse ‘support’ branches, on which an extensive network of fine ‘canopy’ branches bifurcates until most of the host cell volume is filled, generating the characteristic tree-shaped structure². Simultaneously, the plant plasma membrane envelops the growing fungal structure to establish the peri-arbuscular membrane (PAM). Thereby an apoplastic peri-arbuscular space (PAS) is generated between the fungal arbuscular membrane (FAM) and the plant PAM, which has been described as an ‘amorphous’ matrix that is continuous with the host cell wall and contains wall-related macromolecules³. The plant–fungal exchange of nutrients within the arbusculated cell is thought to involve release into the PAS, followed by uptake across either the plant PAM or the FAM.

Plant inorganic phosphate and ammonium transporters with a specific role in arbuscular mycorrhizal symbiosis mediate transport processes at the PAM^{4–6}, whereas equivalent fungal transporters have not been reported. Inorganic phosphate transporters of the rice PT11 type (*Medicago truncatula* PT4⁵) reside in PAM zones surrounding fine arbuscular branches, but are absent from PAM around coarse branches or the trunk^{5,7}. As these transporters mediate most, if not all, symbiotic inorganic phosphate uptake^{8,9}, their PAM distribution pattern indicates functionally distinct membrane

subdomains. Arbuscular establishment is also essential for organic carbon nourishment of the obligate fungal biotroph, to complete its asexual life cycle¹⁰. Being fatty acid heterotrophs¹¹, arbuscular mycorrhizal fungi rely entirely on their plant host for the supply of fatty acids^{12–15}. Conceivably, plant fatty acids ultimately provide the building blocks for the massive de novo fungal plasma membrane biosynthesis associated with the arbuscule, in particular the formation of fine branches (reviewed in ref. ¹⁶). The mechanism by which fatty acids are delivered to the fungus is currently unknown. However, PAM-specific, half-size ABCG transporters Stunted Arbuscule 1 and 2 (STR1 and STR2, respectively) have been proposed as fatty acid exporters in *M. truncatula*¹⁷, suggesting that the uptake of inorganic phosphate and the release of fatty acids may be spatio-temporally linked.

Despite the seemingly huge fungal and plant investment made in producing and accommodating arbuscules, these are ephemeral structures with a lifespan of only 1–2 days in rice¹⁸. Arbuscule development thus reflects an immensely vigorous cell invasion process, brought about by reiterated hyphal bifurcation and elongation that is based on polar hyphal tip growth, common to all filamentous fungi. Senescence of arbuscules resembles the inverse procedure, starting with collapse of fine branches and rapidly proceeding across the more basal parts of the structure until the entire arbuscule has been removed. The window for symbiotic inorganic phosphate uptake (and probably fatty acid release) thus appears restricted to the highly dynamic and short period of fine branch formation.

To capture the ultra-structural detail of plant and fungal membrane surfaces during the successive developmental stages of growing and collapsing arbuscules, we performed transmission electron microscopy (TEM) tomography and three-dimensional (3D) reconstruction on high-pressure-frozen, freeze-substituted rice roots colonized by *R. irregularis*. We found that instead of smoothly aligned, parallel membranes separated by a homogenous interfacial

¹Department of Plant Sciences, University of Cambridge, Cambridge, UK. ²Electron Microscopy Core Facility, University of Heidelberg, Heidelberg, Germany. ³Department of Chemistry, University of Cambridge, Cambridge, UK. ⁴Centre for Organismal Studies, University of Heidelberg, Heidelberg, Germany. ⁵Max-Planck Institute for Terrestrial Microbiology, Marburg, Germany. ⁶Springer Nature Heidelberg, Berlin, Germany. *e-mail: up220@cam.ac.uk

matrix, plant and fungal membranes adopted complex 3D structures. Invasive arbuscular growth was associated with the extensive production of paramural membraneous tubules (memtubs), a structural feature that likewise occurs in maize leaf cell infection by the ear smut fungus *U. maydis*. PAM evaginations populated the PAS, together with extracellular vesicles of plant or fungal origin, throughout all the different stages of arbuscular existence, suggesting not only a further notable increase in contact area between the two symbionts but also sophisticated mechanisms for inter-organismal cell-to-cell communication.

Results

Classification of arbuscular hyphae. Electron microscopically captured images of arbuscules typically show a collection of hyphae which, in micrographs, are distinguishable from rice cortical cell cytosol due to the densely stained fungal cell walls and presence of small circular vacuoles (Supplementary Fig. 1a). To ensure that membrane surfaces in colonized roots were retained as close to their native state as possible, we used high-pressure freezing followed by freeze-substitution to preserve rice root tissue. In chemically fixed rice tissues we consistently observed fixation artefacts corresponding to irregular membrane undulations (Supplementary Fig. 1b). Using this freeze-based method on colonized rice root tissue, we found excellent preservation of fungal and plant membranes while membrane undulations associated with fixation artefacts were not observed (Supplementary Fig. 1c).

With the aim of characterizing plant and fungal membrane details during the arbuscule lifespan, we required a strategy that would accurately discriminate fine arbuscule branches from large hyphal branches and trunk hyphae on TEM cross-section. Trunk and low-order hyphae are visibly larger in diameter than smaller, fine hyphae; however, since arbuscule formation is a continuum of hyphal branching and hyphae are often obliquely sectioned, the identification of fine hyphae based on their diameter alone can be challenging. During filamentous hyphal growth, fungal cell walls become progressively thicker towards the older, more distal part of the fungal hypha as new cell wall material is deposited just behind the growing hyphal tip¹⁹. The fungal cell walls of fine arbuscular branches are typically thinner than in larger mature and arbuscule trunk hyphae^{20,21}. We therefore inferred that fungal cell wall thickness, combined with hyphal diameter, could be used with TEM to distinguish fine from large and trunk hyphae, which is necessary in determining the relative position of a hypha within the arbuscular structure.

Hyphal diameter and cell wall thickness were thus measured from micrographs, while simultaneously visually categorizing hyphae as either fine, large or trunk. Since hyphal cell wall thickness is dependent on the section angle, the thickness of the section and the curvature of the structure, we consistently measured cell wall thickness taken from the thinnest point of the fungal cell wall surrounding a hypha. Selecting hyphae randomly from TEM micrographs, we found a good correlation between hyphal diameter and fungal cell wall thickness (CWT) ($R^2=0.88$, $n=61$ hyphae taken from eight micrographs across seven independent biological replicates). This provided the training dataset and generated a simple linear regression model ($y=42.2 \times \text{CWT} + 131.3$; Supplementary Fig. 2a) with an average mean absolute percentage error of 25% (tested 100-fold using a ratio of 80:20). We next carried out unsupervised *K*-means testing on our training dataset, which identified three clusters that closely matched our visual classification of hyphae as fine, large or trunk (Rand index value = 0.961, Supplementary Fig. 2a). A mean hyphal diameter corresponding to cluster centres of 866.81 nm, 2,058.40 nm and 3,506.82 nm and cell wall thicknesses of 18.76 nm, 47.26 nm and 65.49 nm was obtained for fine, large and trunk hyphae, respectively. An excellent differentiation between fine arbuscule branches and larger trunk hyphae was obtained,

although the distinction between large and trunk hyphae was less clear (Supplementary Fig. 2a). We next determined whether fungal cell wall thickness could be used to predict hyphal diameter together with *K*-means testing to ultimately classify hyphae. A Rand index value of 0.751 (Supplementary Fig. 2b) was obtained. In spite of overlap between large and trunk hyphae, fine arbuscule hyphae were clearly discriminated, indicating that fungal cell wall thickness combined with *K*-means testing can be applied to accurately discriminate fine hyphal branches from large and trunk hyphae in TEM-based analyses.

We frequently observed collapsed hyphae adjacent to viable hyphae (Supplementary Fig. 1a), suggesting that fine arbuscule hyphal branching and collapse are unsynchronized with both simultaneously present in the arbuscule. Collapsed fungal hyphae appeared distorted, with compressed cell walls and mostly devoid of fungal cytoplasm (Supplementary Fig. 1a) as recorded previously²².

Fungal plasma membrane tubules are preferentially associated with fine arbuscular branches.

Unexpectedly, we observed an extensive accumulation of paramural structures in the extracellular space between the fungal plasma membrane and cell wall (Fig. 1a–i). These structures were homogeneous in diameter (49.36 ± 14.3 nm, $n=80$ hyphae taken from eight micrographs across three independent biological replicates) and were delineated by a well-defined lipid bi-layer (Fig. 1b,c). While most appeared vesicular in cross-section, transverse sections revealed that they were membrane tubules (memtubs; Fig. 1a–i). Interestingly, memtubs were not evenly distributed in the paramural space but were clustered together in distinct lateral pockets (Fig. 1a,e,h) or between two fungal protoplasts within a single fungal cell wall (Fig. 1d). This created the impression of a cross-section just above the point of hyphal bifurcation; however, the possibility that memtubs were captured in the inner fold of a bent hypha cannot be excluded. Occasionally, small pockets of memtubs were also observed on the side of thick and trunk branches, which appeared less extensive than those associated with fine branches (Fig. 1f,g). In fully collapsed hyphae, fungal protoplasts were entirely absent whereas memtub-like structures could be found (Fig. 1h,i)²³. However, it was unclear whether these structures corresponded to memtubs or were remnants of the retracting fungal protoplast.

To determine the point during arbuscule growth when memtubs are formed, we measured the frequency with which they occurred in the two hyphal classes, fine and thick (the latter of which included both large and trunk hyphae). Memtubs were observed on 28% of all fine ($n=258$) and on 15% of all thick hyphae ($n=173$), thus significantly more frequently on arbuscular fine branches ($P=0.015$, Supplementary Table 1). The low abundance of memtubs on large and trunk hyphae and their preferential association with thin hyphae suggested that these are probably formed during active growth of arbuscular hyphae but, once formed, persist until hyphal collapse.

Memtubs are continuous with the fungal plasma membrane.

To determine whether memtubs are continuous with the fungal plasma membrane, thereby confirming that they are of fungal origin, and also to gain further insights into their spatial organization, semi-thin sections were generated for TEM tomography. We frequently found memtubs protruding from the fungal plasma membrane into the paramural space (Fig. 2a,b and Supplementary Video 1). Some memtubs remained connected to the fungal cytosol as open tubes (Fig. 2a,f and Supplementary Video 1), while in other cases, narrow constrictions between the memtub and fungal plasma membrane (Fig. 2b,f and Supplementary Video 1) as well as ramifying tubules were observed (Fig. 2f–k and Supplementary Video 1). Interestingly, memtubs appeared highly elongated, forming an interconnecting network of tubules separated by narrow membrane constrictions

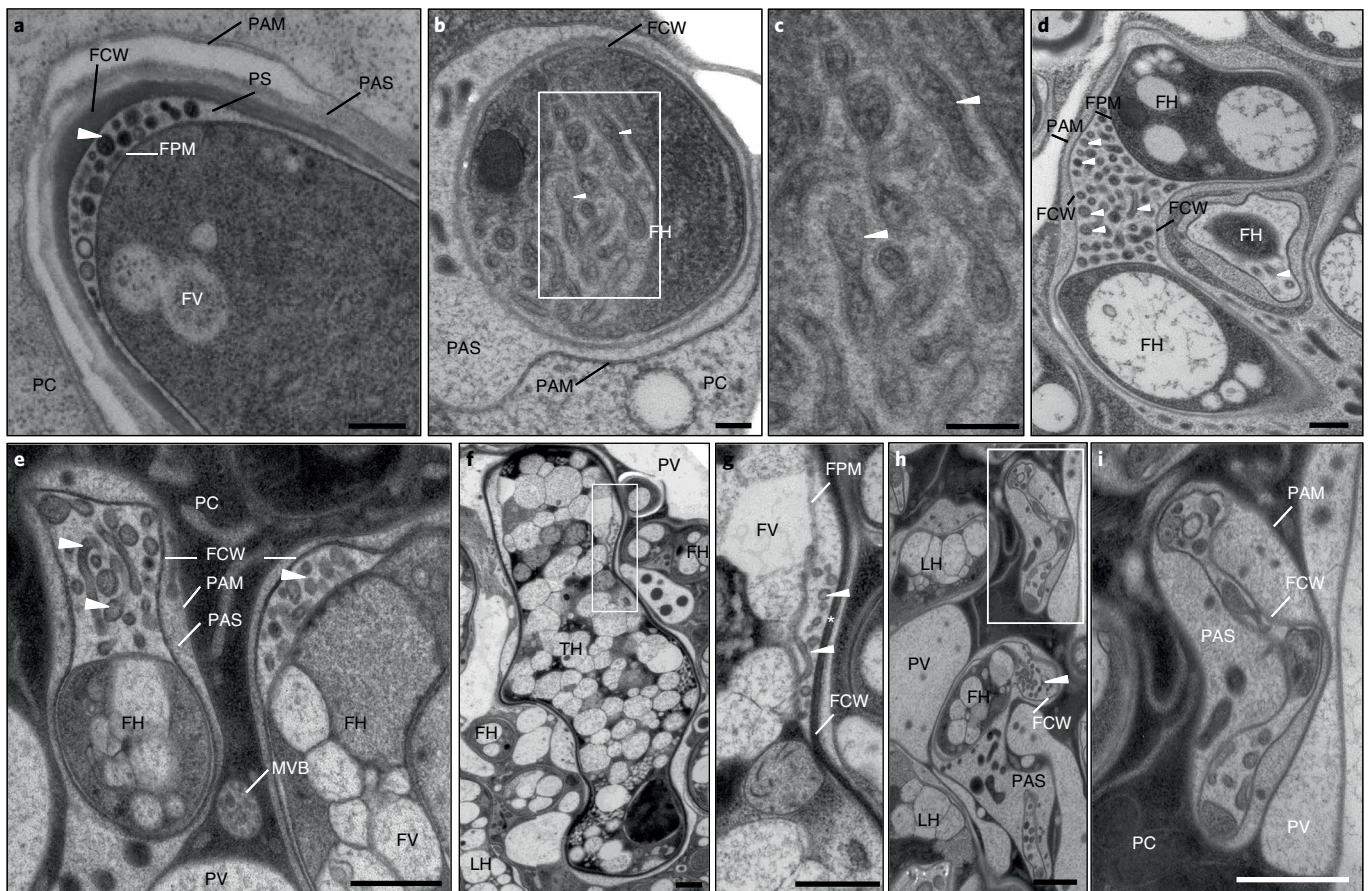


Fig. 1 | Transmission electron micrographs of *Rhizopogon irregularis*-colonized rice cortex cells showing paramural fungal memtubs. a, Fungal memtubs accumulated in the paramural space on the side of a fungal hypha (arrowhead) between the fungal plasma membrane (FPM) and fungal cell wall (FCW). Scale bar, 300 nm. **b**, In the transverse section, memtubs are tubular-vesicular in shape. **c**, Higher magnification of inset in **b** showing memtubs surrounded by a lipid bi-layer (arrowheads). Scale bar, 100 nm. **d**, Memtubs accumulated in the shared paramural space (PS) separating a bifurcating fine hypha (FH; arrowheads) enclosed within a single FCW. Scale bar, 200 nm. **e**, Accumulation of memtubs in a paramural pocket of a FH appearing as extended bulges on the FCW. **f**, Memtubs accumulated in a paramural pocket of a trunk hypha. **g**, Increased magnification of memtubs shown in the inset in **f**. **h**, Overview of FH showing partially collapsed arbuscules and higher magnification of inset in **h** showing the presence of memtub-like structures or a retracting hyphal protoplast in a partially collapsed FH. **e–h**, Scale bar, 500 nm. PAM, peri-arbuscular membrane; PAS, peri-arbuscular space; FV, fungal vacuole; PC, plant cytosol; PV, plant vacuole; LH, large hypha; TH, trunk hypha. Figures are representative of four biological replicates.

(Fig. 2c–e and Supplementary Video 1). Although reminiscent of the budding off of plasma membrane ectosomes, distinctly separate extracellular vesicles were not detected. We additionally found that the open type of memtub joined to form cytoplasmic bridges between two fungal cytosols within a shared fungal cell wall (Fig. 2f–i and Supplementary Video 1). Collectively, we present evidence for the existence of an intricate plasma membrane tubular network and connecting tubules during fine arbuscular hyphal branching.

Fungal memtubs are a conserved feature of invasive hyphal growth. To determine whether memtubs are more broadly associated with arbuscular development in different arbuscular mycorrhizal fungal species, we examined rice roots colonized by *G. rosea*. Membrane tubules similar to those observed for *R. irregularis* were present in the paramural space of a *G. rosea* fine arbuscule hypha (Supplementary Fig. 3a,b) whereas they were absent from large or collapsing hyphae. Moreover, fungal memtubs were also observed in *R. irregularis*- and *Glomus versiforme*-colonized *Brachypodium distachyon* and *M. truncatula*, respectively (Ivanov et al., accompanying manuscript). Therefore, the formation of memtubs consistently appears to coincide with arbuscule development in phylogenetically distant AM fungi.

We next investigated whether memtubs are a generic feature associated with invasive growth of arbuscular mycorrhizal fungal hyphae. Rice root colonization by *R. irregularis* involves hyphal spread in the intercellular space, which precedes and accompanies intracellular arbuscular development in the cortex. Although rarely observed (Supplementary Table 1), memtubs also occurred in paramural pockets on intercellular hyphae, wedged between plant and fungal cell walls (Supplementary Fig. 4a,b). Memtubs are therefore not an exclusive feature of arbuscular hyphae.

To determine the extent to which memtub formation is more broadly associated with invasive hyphal growth in a taxonomically distant fungus, we performed TEM analysis on maize leaf sheath tissue colonized by the corn smut fungal pathogen *U. maydis*. Tissue was collected at 1–2 days post-inoculation (dpi) to capture the stage of early appressorial penetration of the leaf epidermis³⁴. Tubular vesicular membrane structures resembling memtubs were found in the paramural space of a young penetrating fungal hypha (Supplementary Fig. 5). The presence of memtubs during the early stage of cellular infection by *U. maydis* indicated that these are formed during invasive fungal hyphal growth in both beneficial and pathogenic filamentous fungi.

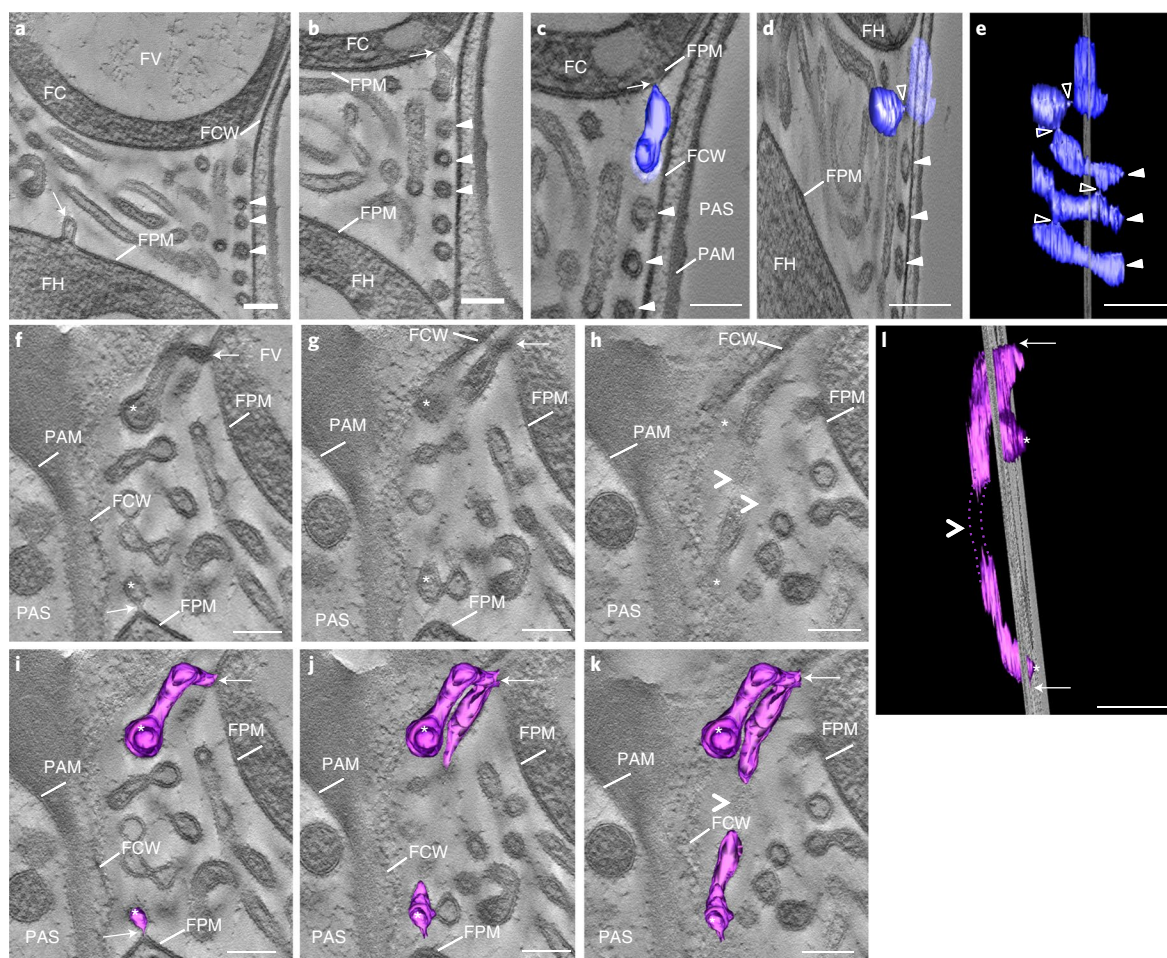


Fig. 2 | Tomography and 3D reconstruction of fungal memtubs. a, Single optical tomography slices showing memtubs formed by budding from the fungal plasma membrane (FPM, arrow). Memtubs appear both vesicular and tubular in shape (white arrowheads). **b**, A narrow constriction between the FPM and a memtub (arrow) can be seen. **c**, Corresponding 3D reconstruction of **b** showing the narrow constriction between the FPM and memtub (white arrow). **d**, Tilted view of **c** showing the presence of a second memtub separated from the memtub shown in **c** (transparent view) by a narrow constriction (open arrowhead). **e**, 3D reconstruction of **b** confirming that memtubs are tubular in shape rather than spherical (filled arrowheads), and appear interconnected by narrow constrictions (open arrowheads). **f-h**, Digital tomography serial sections and respective 3D reconstruction (**i-l**) showing two open types of memtubs (indicated by asterisks) originating from opposite ends of a bifurcating fungal hypha and aligned with one another. **h-k**, An underlying shadow (arrowhead) suggests that the marked memtubs are interconnected. **l**, Tilted side view of **k** showing putative interconnected memtubs (magenta, stippled lines). Abbreviations as in Fig. 1. Scale bar, 100 nm. Tomogram was produced from a representative sample of four biological replicates.

PAM protrusions and membrane-bound vesicular structures occur in the PAS. It is generally assumed that the PAM envelops the arbuscule like a glove; however, our TEM analysis of *R. irregularis*-colonized rice cortical cells reproducibly showed that the PAM enclosed an apoplastic PAS of variable size, often surrounding more than one fungal hypha (Fig. 3a,b). The PAS has previously been described as an amorphous, and therefore somewhat ‘neutral’, matrix³. Our TEM approach, however, revealed that, in addition, the PAS contains an extensive number of membrane-bound structures of heterogeneous shape and size (Fig. 3a-d), adding to membrane complexity. We distinguished sophisticated, swirl-like PAM evaginations (Fig. 3a,b and Supplementary Video 2) and vesicular-like, membrane-bound structures (Fig. 3c and Supplementary Video 2). In contrast to the fungal memtubs, the diameter of the PAS structures varied widely, spanning two orders of magnitude from ~30 to ~3,000 nm. In addition, the vesicular structures differed in electron density, suggesting that these are heterogeneous (Fig. 3c).

The symbiosis-specific rice inorganic phosphate transporter PT11 uniquely localizes to the PAM subdomain surrounding expanding fine branches and is therefore expected to be present

on the observed PAM evaginations. To validate the association of PAS internal vesicular structures with fine arbuscular branches, we performed immunogold labelling (IGL) on PT11-green fluorescent protein (GFP)-expressing rice plants using anti-GFP antibody. Immunogold particles localized only to the PAM and to a few vesicular structures within the PAS of transgenic roots (Supplementary Fig. 6a,b), thereby indicating that a fraction of the vesicular structures was derived from the PAM of fine hyphal branches during symbiotic inorganic phosphate uptake. To establish the frequency with which vesicular structures accumulated around all hyphal types, we determined their occurrence within the PAS of fine and thick (large and trunk, respectively) hyphae. Overall, a significantly higher number of hyphae was associated with vesicular structures as compared to memtubs (53%, $n = 431$, $P = 3.938 \times 10^{-10}$; Supplementary Table 1). No significant difference was observed in the frequency with which vesicular structures accumulated around fine (52%, $n = 258$) as opposed to large/trunk (54%, $n = 173$) hyphae, indicating that these are ubiquitously produced during arbuscule formation. Interestingly, vesicular structures were also found in the PAS surrounding collapsing fine branches, often appearing smaller

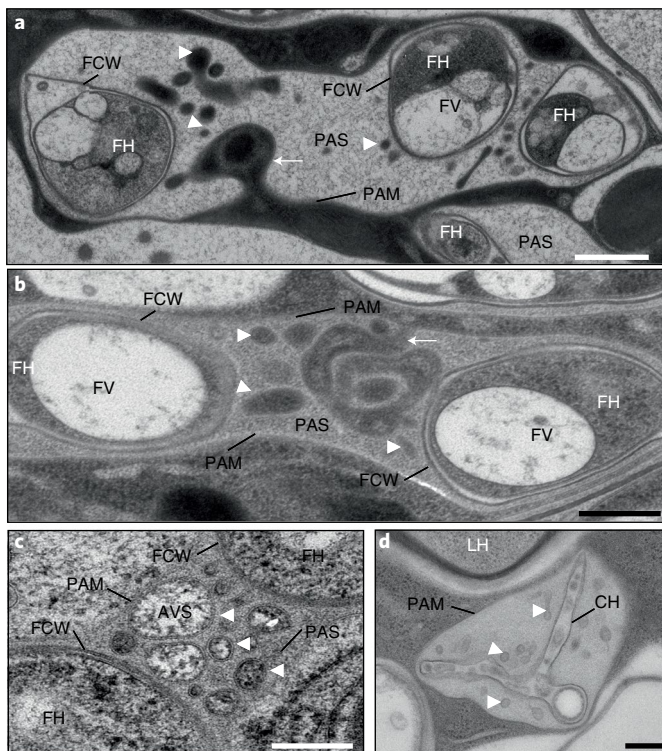


Fig. 3 | Transmission electron micrographs documenting PAM evaginations and membrane-bound vesicles within the PAS. **a**, A large PAS surrounds numerous fine arbuscular hyphae, tubular apoplastic vesicular structures (AVS; arrowheads; scale bar, 500 nm), as well as swirl-like evaginations of the PAM (**b**, arrow; scale bar, 300 nm). **c**, The lipid bi-layer surrounding the AVS indicates that these are membrane-bound (arrowheads); AVS are heterogeneous both in size and electron density. **d**, Membrane-bound AVS (arrowheads) are present in the PAS enclosing collapsing fine fungal hyphae. **c,d**, Scale bar, 200 nm. FCW, fungal cell wall, FPM, fungal plasma membrane. Other abbreviations as in Fig. 1. Figures are representative of four biological replicates.

in size and less electron-dense compared to those present around intact hyphae (Fig. 3d), which may be linked to reduced membrane deposition as the branch begins to collapse. Vesicular structures therefore remain associated with arbuscular hyphal branches throughout formation and collapse.

To determine whether vesicular structures are a widespread feature of arbuscular mycorrhizal symbiosis, we examined the PAS of *G. rosea*-colonized rice cells. An accumulation of membranous bodies that were similarly delineated by a clear lipid bi-layer, and that appeared heterogeneous in size, shape and electron density, were also observed (Supplementary Fig. 3a,b). The similarity in appearance of PAS internal structures in the roots of *R. irregularis*- and *G. rosea*-infected rice and *R. irregularis*- and *G. versiforme*-colonized *M. truncatula* (Ivanov et al., accompanying paper) suggested the presence of common membrane remodelling mechanisms during cell invasion of diverse plant species by these distantly related arbuscular mycorrhizal fungi.

PAS-localized vesicular structures consist of PAM-connected, interconnected and separate extracellular vesicles. To determine whether vesicular structures are connected to the PAM as we previously observed for fungal memtubs, or would also include separate extracellular bodies, we performed TEM tomography and 3D reconstruction using IMOD software (Fig. 4a–l and Supplementary Video 2). In the PAS around thin arbuscular branches we observed

vesicles that were either separate from the PAM but linked with one another, containing narrow, stalk-like connections (Fig. 4a–d and Supplementary Video 2), or appeared as free individual units of extracellular vesicles (Fig. 4a–f and Supplementary Video 2). Although the presence of imaging artefacts cannot be excluded with certainty, the appearance of extracellular vesicles resembled that of structures observed in other plant–fungus interactions^{25–27}. Further support for the occurrence of extracellular vesicles is provided by the observation of similar structures in the PAS surrounding arbuscules of *G. versiforme* in *M. truncatula* cortical cells (Ivanov et al., accompanying paper). In addition, tomography captured a PAM-continuous evagination in the same PAS, which also showed a notable constriction between the PAM and the more vesicular part (Fig. 4g–l and Supplementary Video 2). In contrast to memtubs, tubular connections between various neighbouring PAMs were not observed. In summary, diverse types of membrane structures populate the PAS, including PAM evaginations of variable size and shape and single or clustered interconnected extracellular vesicles, consistent with their role in intercellular communication.

Multi-vesicular bodies fuse with the PAM. The release of extracellular vesicles into the apoplast can result from either vesicles budding off from the plasma membrane (ectosomes) or fusion of multi-vesicular bodies (MVBs) with the plasma membrane (exosomes)³⁸. Either mechanism may be involved in the generation of extracellular vesicles in the PAS. On the one hand, the narrow constrictions observed on PAS vesicular bodies would suggest that pinching off may occur. On the other hand, we frequently found MVBs in the host cytoplasm in proximity to fungal hyphae (Supplementary Fig. 7a), and also observed plant MVBs that appeared to have fused with the PAM in areas where vesicular structures were found in the adjacent PAS (Supplementary Fig. 7b), thereby suggesting that the MVB pathway may contribute to extracellular vesicle secretion.

Discussion

During arbuscule formation, the switch from lower- to higher-order hyphal branching generates a dramatically increased surface area where symbiotic nutrient exchange occurs. We found highly elongated fungal tubular membrane structures in spatially restricted paramural pockets on opposite sides of thin-walled small hyphae, or juxtaposed between interconnected hyphae that appeared bifurcated, with two fungal protoplasts surrounded by a single fungal cell wall. The presence of memtubs between two fungal hyphae and their infrequent association with larger hyphae would argue against a role for memtubs in hyphal tip growth. Conceivably, memtubs could increase the absorptive surface area for the acquisition of plant-derived compounds that could diffuse through the fungal cell wall. By analogy, in the giant alga *Chara corallina* a positive correlation was found between the rate of chloride influx and the associated increase in membrane surface area via an interconnected membrane tubular network, termed charasomes^{29,30}. We favour, however, the scenario where memtubs would be involved in the release of molecules that modulate their surroundings to facilitate hyphal growth, and perhaps also the secretion of fungal effectors to manipulate the host cell. Although we were unable to detect shedding of micro-vesicles from memtubs, the delivery of ‘bioactive cargo’ via extracellular vesicles cannot be excluded. Memtubs are predominantly associated with hyphal forks and lateral pockets of single hyphae. The spatiotemporal relationship between the two patterns is unclear: for instance, is memtub occurrence in lateral pockets a remnant of hyphal branching?

Paramural vesicles from arbuscular mycorrhizal fungi were reported as early as 1961 (ref. ³¹), and repeatedly since then for a range of different arbuscular mycorrhizal fungal species^{32–37}. However, in the absence of 3D tomography, their organization into tubular networks continuous with the FPM has been largely

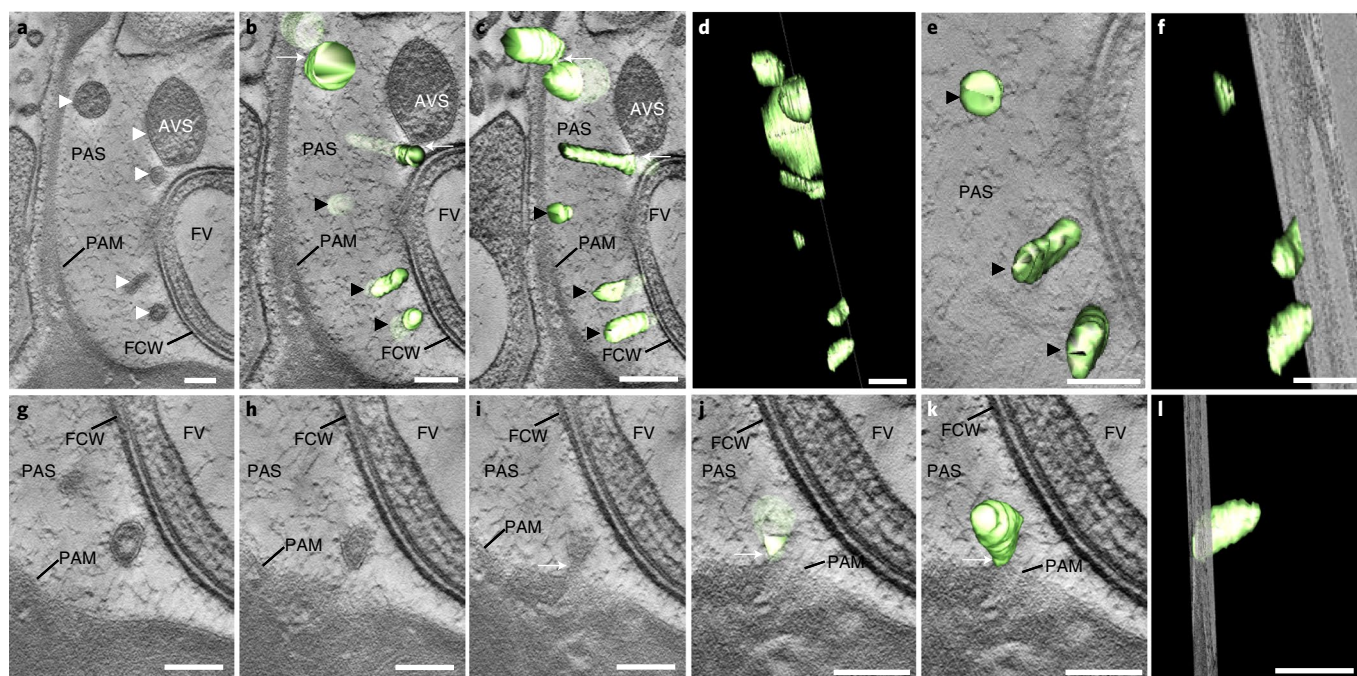


Fig. 4 | Tomography and 3D reconstruction of PAS-localized apoplastic vesicular structures. **a**, Single optical slice of a tomogram showing an overview of apoplastic vesicular structures (AVS) in the PAS (white arrowheads). **b–f**, 3D reconstruction of **a** showing several AVS appearing as either separate (black arrowheads) or interconnected (white arrows); 3D perspective of the top (**b**) and bottom (**c**) of the tomography slice shown in **a**. **d**, Tilted side view and 3D reconstruction of all vesicular structures shown in **a**. **e, f**, Top (**e**) and side (**f**) views of the tilted tomogram showing separate vesicular structures. **g–i**, Optical serial sections through a vesicular PAM evagination. **j–l**, 3D reconstruction of the bottom (**j**), top (**k**) and tilted (**l**) tomogram showing side view of the AVS shown in **g–i**, which appears to be derived by evagination from the PAM. Abbreviations as in Fig. 1. Scale bar, 100 nm. Tomogram was produced from a representative sample of four biological replicates.

overlooked. Since memtubs are present not only during cell invasion by various arbuscular mycorrhizal fungi but also in the ear smut fungus *U. maydis*, we hypothesize the existence of a generic role during invasive hyphal growth in nutrient-rich environments. Indeed, published reports of saprophytic filamentous fungi provide two-dimensional (2D) documentation of membrane tubular structures within the paramural space of axenically growing hyphae³², which resemble the memtubs described here for arbuscular mycorrhizal fungi and were called lomasomes/plasmalemmasomes. The formation of memtubs thus appears associated with expanding absorptive hyphae during both saprophytic and biotrophic filamentous growth, including intracellular host invasion in parasitic and mutualistic plant–fungal interactions.

In addition, we documented the accumulation of extracellular vesicles within the PAS surrounding arbuscular hyphae. These were of different electron density, which may indicate either their heterogeneous cargo or, alternatively, their heterogeneous origin, being either plant or fungus derived. Although at this point in time we cannot provide experimental evidence, it is possible that the fungus releases extracellular vesicles into the PAS.

Extracellular vesicles have been described as consisting of both ectosomes and exosomes that facilitate both intercellular and inter-species communication²⁷ (reviewed in ref. ³⁸). The nature of PAS internal extracellular vesicles is presently unclear, because the vesicular constrictions of PAM evaginations are similar to the stage just before pinching off of the vesicle. PT11-eGFP signalling on vesicular structures within the PAS would be consistent with ectosomes that had budded off the PAM; however, according to 2D IGL imaging, the distinction between free and connected vesicles cannot be made. Our finding is in agreement with previous reports on localization of the symbiotic H⁺ATPase to the PAM and to membranous vesicles present in the PAS^{39–41}. However, because the

documentation referred to here was limited to 2D IGL, the distinction between free and attached membrane structures could not be verified. Extracellular vesicles that resemble ectosomes were also detected in *Glomus mosseae* colonization of various plant species, as well as in fine arbuscular hyphae from natural inocula⁴², suggesting that these are ubiquitously produced during fine arbuscular branching, which is consistent with our observation that extracellular vesicles are present in the association between rice and *G. rosea*.

In addition to accumulation of MVBs around arbuscular hyphae, we observed that the former appeared to fuse with the PAM, thereby confirming the potential release of exosomes during arbuscule formation. Some of the host cytoplasm would thus be transferred into the PAS, including nucleic acids, proteins and nutrients. In plant–pathogen interactions, extracellular vesicles corresponding to exosomes accumulated at sites where the formation of early defence structures, namely cell wall appositions, had occurred^{25,26}. Exosomes were also present in the extra-haustorial matrix of the biotrophic powdery mildew pathogens *Golovinomyces orontii* and *Arabidopsis thaliana*⁴³. Moreover, proteome analysis of extracellular vesicle cargo from the apoplast of *A. thaliana* and sunflower showed that extracellular vesicles were enriched by a diverse range of stress and defence proteins, confirming an involvement of exosomes in innate immunity and intercellular communication^{44,45}. In addition, only 16% of proteins present in extracellular vesicles had signal peptides, suggesting a role for the vesicles in non-canonical secretion⁴⁴.

Importantly, recent studies have shown that fungi are capable of taking up host extracellular vesicles; for instance, spores of the phytopathogenic fungus *Sclerotinia sclerotium* were able to take up extracellular vesicles isolated from sunflower, causing a suppression of fungal growth⁴⁵. Similarly, *A. thaliana* extracellular vesicles containing small RNAs (sRNAs) were acquired at infection sites by the fungal pathogen *Botrytis cinerea*²⁷, demonstrating a role for plant

extracellular vesicles in inter-kingdom communication to combat the invading microbe, more specifically in host-induced gene silencing. Interestingly, host-induced silencing of the gene *R. irregularis* *Monosaccharide Transporter 2* in *M. truncatula* confirmed that, in arbuscular mycorrhizal symbiosis, plants transfer small interfering RNAs to arbuscular mycorrhizal fungi⁴⁶; however, no involvement of extracellular vesicles was demonstrated.

In summary, our study provides an ultra-structural 3D reconstruction of the hitherto poorly understood dynamic and spatial reorganization of plant and fungal membranes, and of the ephemeral PAS during the lifespan of the arbuscule. Future identification of extracellular vesicle proteins and cargo in arbuscule formation and collapse will provide exciting and novel insights into the host–fungal relationship at the PAS, and uncover novel mechanisms of arbuscular function.

Methods

Plant and fungal material. Seven-day-old maize inbred line *Zea mays* (L.) (corn) seedlings of the variety Early Golden Bantam (Olds Seeds), and 2- to 3-week-old *Oryza sativa* ssp. japonica cv. Nipponbare wild-type and transgenic rice lines carrying *PromPT11:PT11-eGFP*⁷, were used in this study. For rice inoculation with beneficial fungi, de-husked seeds were surface-sterilized in 3% hypochlorite solution and pre-germinated on 0.3% Bacto-agar plates for 4 days at 30 °C in the dark. Germinated seedlings were transferred to 60 mm Petri dishes containing untransformed Nipponbare rice, which were colonized by either *R. irregularis* or *G. rosea* and used at 6 weeks post-inoculation, thus functioning as high-inoculum strength ‘nurse plants’. Plants were nurtured in a growth chamber with a 12 h/12 h day/night cycle at 28/22 °C and 60% humidity. Plants were fertilized every second day with half-strength Hoagland solution, containing 25 μM KH₂PO₄. Seedlings were harvested for imaging at 10 dpi.

For infection of maize with *U. maydis*, the solopathogenic strain ULL152 (SG200Suc2AvitagHA-Pcmu1-GFP-Avitag HA) was generated. This strain expresses enhanced GFP (eGFP) from the strong *cmu1* promoter. The *cmu1* promoter is induced after colonization⁴⁷, and concomitant cytoplasmic eGFP expression facilitates the detection of biotrophic hyphae. To construct the strain, plasmid pLL188 was generated by cloning eGFP into pLL181, a derivative of p123 that contains the *cmu1* promoter and AvitagHA (Presti, unpublished). To this end, eGFP was amplified using OLL258 (BamHI site, primer sequence ttttGGATCCATGGTGAGCAAGGGCGAG) and OLL499 (XbaI site, primer sequence: ttttTCTAGACTTGTACAGCTCGTCCATGCC), digested with BamHI/XbaI and ligated to BamHI/XbaI-digested pLL181. pLL188 was then linearized with Ssp1 and integrated into the *ip* locus of strain ULL152 (ref. ⁴⁸). For the infection of maize seedlings, the protocol described in ref. ²⁴ was followed. Seven-day-old seedlings were used, and infected leaf samples for microscopy were harvested at 2 dpi, a stage when penetration had occurred and biotrophic hyphae were established.

Sample preparation for TEM and IGL. Ultra-structural analyses of arbuscule-containing cells in *R. irregularis*-colonized rice roots are largely hindered by physical barriers of mature tissue such as thick cell walls, suberized sclerenchyma layer and extensive aerenchyma that slow penetration of chemical fixatives, resulting in ultra-structural artefacts (reviewed in ref. ⁴⁹). Therefore, to overcome these physical barriers to rice tissue preservation, we used young seedlings at 10 days post germination (dpg) for TEM analysis. For chemical fixation, 1–2 mm root sections were fixed in 1.5% paraformaldehyde/0.5% glutaraldehyde in 50 mM cacodylate buffer (pH7.4). Samples were post-fixed in 1% OsO₄ followed by en bloc staining in 0.5% uranyl acetate and serial dehydration in acetone, and then embedded in Spurr’s resin. For high-pressure freezing, samples were excised into 1 mm sectors in 1-hexadecene and immediately vacuum-infiltrated in a solution used for protection against freezing (200 mM sucrose, 10 mM trehalose, 10 mM Tris Buffer, pH6.6) for approximately 1 min before transfer to aluminium planchettes (types 241 and 242, GmbH). High-pressure freezing was carried out with a Baltec HPM010 (Bal-Tec) and samples stored in liquid nitrogen until further use. Freeze-substitution was carried out as described previously⁵⁰.

Tomography and 3D modelling. For electron tomography, 250 nm sections were placed on formvar-coated copper slotgrids, counterstained and placed in a high-tilt holder (Model 2040; Fischione Instruments). The area of interest was recorded on a Tecnai F20 EM (FEI), operating at 200 kV using the SerialEM software package (Mastrorade 2005). Images were taken at every degree over a range ±60° range on a FEI Eagle 4K×4K CCD camera at a magnification of ×19,000 and a binning of 2 (pixel size 1.13 nm). Tilted images were aligned by using the positions of the fiducial gold particles. Tomograms were generated using the *R*-weighted back-projection algorithm. These were displayed as slices one voxel thick; vesicles were modelled and analysed with the IMOD software package⁵¹.

Quantitative analysis and modelling. To compute the model for hyphal diameter and fungal cell wall thickness, the data were randomly split into test and training datasets at a ratio of 20:80. The operation was repeated 100 times and the average mean absolute percentage error was calculated. Splitting and prediction were performed using the caret package.

The first step in cluster analysis was cluster number determination. R package factoextra (factoextra: Extract and Visualize the Results of Multivariate Data Analyses. R package version 1.0.5.) was employed to apply the silhouette method. For cluster determination, base R function *kmeans* was used. For the calculation of Rand index, the function *arandi* from R package mcclust (mcclust: Process an MCMC Sample of Clusterings. R package version 1.0.) was applied. All plots were drawn using the package ggplot2 (ggplot2: Elegant Graphics for Data Analysis, Springer-Verlag). Statistical analysis of the frequency at which membrane structures accumulate across fungal hyphae tested was done by Fisher test.

Reporting Summary. Further information on research design is available in the Nature Research Reporting Summary linked to this article.

Data availability

All data that support the findings of this study are available from the corresponding author on request.

Received: 15 August 2018; Accepted: 8 January 2019;

Published online: 8 February 2019

References

- Choi, J., Summers, W. & Paszkowski, U. Mechanisms underlying establishment of arbuscular mycorrhizal symbioses. *Annu. Rev. Phytopathol.* **56**, 135–160 (2018).
- Gutjahr, C. & Parniske, M. Cell biology: control of partner lifetime in a plant–fungus relationship. *Curr. Biol.* **27**, R420–R423 (2017).
- Balestrini, R., Hahn, M. G., Faccio, A., Mendgen, K. & Bonfante, P. Differential localization of carbohydrate epitopes in plant cell walls in the presence and absence of arbuscular mycorrhizal fungi. *Plant Physiol.* **111**, 203–213 (1996).
- Paszkowski, U., Kroken, S., Roux, C. & Briggs, S. P. Rice phosphate transporters include an evolutionarily divergent gene specifically activated in arbuscular mycorrhizal symbiosis. *Proc. Natl Acad. Sci. USA* **99**, 13324–13329 (2002).
- Harrison, M. J., Dewbre, G. R. & Liu, J. A phosphate transporter from *Medicago truncatula* involved in the acquisition of phosphate released by arbuscular mycorrhizal fungi. *Plant Cell* **14**, 2413–2429 (2002).
- Breullin-Sessoms, F. et al. Suppression of arbuscule degeneration in *Medicago truncatula* phosphate transporter4 mutants is dependent on the ammonium transporter 2 family protein AMT2;3. *Plant Cell* **27**, 1352–1366 (2015).
- Kobae, Y. & Hata, S. Dynamics of periarbuscular membranes visualized with a fluorescent phosphate transporter in arbuscular mycorrhizal roots of rice. *Plant Cell Physiol.* **51**, 341–353 (2010).
- Javot, H., Pumplin, N. & Harrison, M. J. Phosphate in the arbuscular mycorrhizal symbiosis: transport properties and regulatory roles. *Plant Cell Environ.* **30**, 310–322 (2007).
- Yang, S. Y. et al. Nonredundant regulation of rice arbuscular mycorrhizal symbiosis by two members of the phosphate transporter1 gene family. *Plant Cell* **24**, 4236–4251 (2012).
- Roth, R. & Paszkowski, U. Plant carbon nourishment of arbuscular mycorrhizal fungi. *Curr. Opin. Plant Biol.* **39**, 50–56 (2017).
- Wewer, V., Brands, M. & Dormann, P. Fatty acid synthesis and lipid metabolism in the obligate biotrophic fungus *Rhizophagus irregularis* during mycorrhization of *Lotus japonicus*. *Plant J.* **79**, 398–412 (2014).
- Bravo, A., Brands, M., Wewer, V., Dormann, P. & Harrison, M. J. Arbuscular mycorrhiza-specific enzymes fatm and ram2 fine-tune lipid biosynthesis to promote development of arbuscular mycorrhiza. *New Phytol.* **214**, 1631–1645 (2017).
- Luginbuehl, L. H. et al. Fatty acids in arbuscular mycorrhizal fungi are synthesized by the host plant. *Science* **356**, 1175–1178 (2017).
- Jiang, Y. et al. Plants transfer lipids to sustain colonization by mutualistic mycorrhizal and parasitic fungi. *Science* **356**, 1172–1175 (2017).
- Keymer, A. et al. Lipid transfer from plants to arbuscular mycorrhiza fungi. *eLife* **6**, e29107 (2017).
- Keymer, A. & Gutjahr, C. Cross-kingdom lipid transfer in arbuscular mycorrhiza symbiosis and beyond. *Curr. Opin. Plant Biol.* **44**, 137–144 (2018).
- Zhang, Q., Blaylock, L. A. & Harrison, M. J. Two *Medicago truncatula* half-ABC transporters are essential for arbuscule development in arbuscular mycorrhizal symbiosis. *Plant Cell* **22**, 1483–1497 (2010).
- Kobae, Y. & Fujiwara, T. Earliest colonization events of *Rhizophagus irregularis* in rice roots occur preferentially in previously uncolonized cells. *Plant Cell Physiol.* **55**, 1497–1510 (2014).
- Girbardt, M. Über die Substruktur von *Polystictus versicolor* L. *Arch. Mikrobiol.* **28**, 255–269 (1958).

20. Bonfanteasolo, P., Grippiolo, R. & Scannerini, S. Light and electron-microscopic features of the vesicular-arbuscular mycorrhiza in vitis roots. *Caryologia* **32**, 120–120 (1979).
21. Gianinazzepearson, V. & Gianinazzi, S. Cellular and genetic aspects of interactions between hosts and fungal symbionts in mycorrhizae. *Genome* **31**, 336–341 (1989).
22. Cox, G. & Sanders, F. Ultrastructure of host-fungus interface in a vesicular-arbuscular mycorrhiza. *New Phytol.* **73**, 901–90 (1974).
23. Ivanov, S. et al. *Nat. Plants* <https://doi.org/10.1038/s41477-019-0364-5> (2019).
24. Lanver, D. et al. The biotrophic development of *Ustilago maydis* studied by rna-seq analysis. *Plant Cell* **30**, 300–323 (2018).
25. An, Q., Ehlers, K., Kogel, K. H., van Bel, A. J. & Huckelhoven, R. Multivesicular compartments proliferate in susceptible and resistant MLA12-barley leaves in response to infection by the biotrophic powdery mildew fungus. *New Phytol.* **172**, 563–576 (2006).
26. An, Q., Huckelhoven, R., Kogel, K. H. & van Bel, A. J. Multivesicular bodies participate in a cell wall-associated defence response in barley leaves attacked by the pathogenic powdery mildew fungus. *Cell Microbiol.* **8**, 1009–1019 (2006).
27. Cai, Q. et al. Plants send small RNAs in extracellular vesicles to fungal pathogen to silence virulence genes. *Science* **360**, 1126–1129 (2018).
28. Cocucci, E. & Meldolesi, J. Ectosomes and exosomes: shedding the confusion between extracellular vesicles. *Trends Cell Biol.* **25**, 364–372 (2015).
29. Barton, R. Electron microscope studies on surface activity in cells of chara vulgaris. *Planta* **66**, 95–105 (1965).
30. Lucas, W. J., Keifer, D. W. & Pesacreta, T. C. Influence of culture-medium pH on charasome development and chloride transport in chara-coralina. *Protoplasma* **130**, 5–11 (1986).
31. Moore, R. T. & McAlear, J. H. Fine structure of mycota. 5. Lomasomes—previously uncharacterized hyphal structures. *Mycologia* **53**, 194–19 (1961).
32. Marchant, R. & Moore, R. T. Lomasomes and plasmalemmasomes in fungi. *Protoplasma* **76**, 235–247 (1973).
33. Pigott, C. D. Fine-structure of mycorrhiza formed by cenococcum-geophilum fr on tilia-cordata mill. *New Phytol.* **92**, 501–512 (1982).
34. Heath, I. B. & Greenwo, Ad Structure and formation of lomasomes. *J. Gen. Microbiol.* **62**, 129–12 (1970).
35. Bracker, C. E. Ultrastructure of fungi. *Annu. Rev. Phytopathol.* **5**, 343–34 (1967).
36. Dexheimer, J., Gianinazzi, S. & Gianinazzepearson, V. Ultrastructural cytochemistry of the host-fungus interfaces in the endomycorrhizal association *Glomus mosseae*-*Allium cepa*. *Pflanzenphysiol.* **92**, 191–206 (1979).
37. Scannerini, S. & Bonfanteasolo, P. Comparative ultrastructural analysis of mycorrhizal associations. *Can. J. Bot.* **61**, 917–943 (1983).
38. Lefebvre, F. A. & Lecuyer, E. Small luggage for a long journey: transfer of vesicle-enclosed small RNA in interspecies communication. *Front. Microbiol.* **8**, 377 (2017).
39. Marx, C., Dexheimer, J., Gianinazzepearson, V. & Gianinazzi, S. Enzymatic studies on the metabolism of vesicular-arbuscular mycorrhizas. 4. Ultracytoenzymological evidence (atpase) for active transfer processes in the host-arbuscule interface. *New Phytol.* **90**, 37–43 (1982).
40. Gianinazzepearson, V., Smith, S. E., Gianinazzi, S. & Smith, F. A. Enzymatic studies on the metabolism of vesicular arbuscular mycorrhizas. 5. Is h⁺-atpase a component of atp-hydrolyzing enzyme-activities in plant fungus interfaces? *New Phytol.* **117**, 61–74 (1991).
41. Gianinazzi-Pearson, V., Arnould, C., Oufattole, M., Arango, M. & Gianinazzi, S. Differential activation of H⁺-ATPase genes by an arbuscular mycorrhizal fungus in root cells of transgenic tobacco. *Planta* **211**, 609–613 (2000).
42. Dexheimer, J., Marx, C., Gianinazzepearson, V. & Gianinazzi, S. Ultracytological studies of plasmalemma formations produced by host and fungus in vesiculararbuscular mycorrhizae. *Cytologia* **50**, 461–471 (1985).
43. Micali, C. O., Neumann, U., Grunewald, D., Panstruga, R. & O'Connell, R. Biogenesis of a specialized plant-fungal interface during host cell internalization of *Golovinomyces orontii* haustoria. *Cell Microbiol.* **13**, 210–226 (2011).
44. Rutter, B. D. & Innes, R. W. Extracellular vesicles isolated from the leaf apoplast carry stress-response proteins. *Plant Physiol.* **173**, 728–741 (2017).
45. Regente, M. et al. Plant extracellular vesicles are incorporated by a fungal pathogen and inhibit its growth. *J. Exp. Bot.* **68**, 5485–5495 (2017).
46. Helber, N. et al. A versatile monosaccharide transporter that operates in the arbuscular mycorrhizal fungus *Glomus* sp. is crucial for the symbiotic relationship with plants. *Plant Cell* **23**, 3812–3823 (2011).
47. Djamei, A. et al. Metabolic priming by a secreted fungal effector. *Nature* **478**, 395–398 (2011).
48. Lo Presti, L. et al. An assay for entry of secreted fungal effectors into plant cells. *New Phytol.* **213**, 956–964 (2017).
49. McDonald, K. L. & Auer, M. High-pressure freezing, cellular tomography, and structural cell biology. *Biotechniques* **41**, 137 (2006).
50. Hillmer, S., Viotti, C. & Robinson, D. G. An improved procedure for low-temperature embedding of high-pressure frozen and freeze-substituted plant tissues resulting in excellent structural preservation and contrast. *J. Microsc.* **247**, 43–47 (2012).
51. Kremer, J. R., Mastronarde, D. N. & McIntosh, J. R. Computer visualization of three-dimensional image data using IMOD. *J. Struct. Biol.* **116**, 71–76 (1996).

Acknowledgements

We thank A. Bates and S. Gold for technical assistance, and Y. Kobae for kindly providing PT11-GFP transgenic rice lines. R. Roth was supported by Marie Curie FP7-PEOPLE-2013-IEF grant No. 629887 and by the Isaac Newton Trust RG74108; and U. Paszkowski by the BBSRC grant No. BB/N008723/1.

Author contributions

R.R. and U.P. conceptualized the project. R.R., S.H. and C.F. carried out the experiments. R.R. and S.H. conducted the TEM and IGL analysis. C.F. and S.H. carried out the tomography and R.R. performed the IMOD 3D reconstruction. R.R. and M.C. did the quantitative analysis. R.R. and U.P. wrote the manuscript.

Competing interests

The authors declare no competing interests.

Additional information

Supplementary information is available for this paper at <https://doi.org/10.1038/s41477-019-0365-4>.

Reprints and permissions information is available at www.nature.com/reprints.

Correspondence and requests for materials should be addressed to U.P.

Journal Peer Review Information Nature Plants thanks Rogers Innes, Erik Limpens and other anonymous reviewers for their contribution to the peer review of this work.

Publisher's note: Springer Nature remains neutral with regard to jurisdictional claims in published maps and institutional affiliations.

© The Author(s), under exclusive licence to Springer Nature Limited 2019

Reporting Summary

Nature Research wishes to improve the reproducibility of the work that we publish. This form provides structure for consistency and transparency in reporting. For further information on Nature Research policies, see [Authors & Referees](#) and the [Editorial Policy Checklist](#).

Statistical parameters

When statistical analyses are reported, confirm that the following items are present in the relevant location (e.g. figure legend, table legend, main text, or Methods section).

n/a Confirmed

- The exact sample size (n) for each experimental group/condition, given as a discrete number and unit of measurement
- An indication of whether measurements were taken from distinct samples or whether the same sample was measured repeatedly
- The statistical test(s) used AND whether they are one- or two-sided
Only common tests should be described solely by name; describe more complex techniques in the Methods section.
- A description of all covariates tested
- A description of any assumptions or corrections, such as tests of normality and adjustment for multiple comparisons
- A full description of the statistics including central tendency (e.g. means) or other basic estimates (e.g. regression coefficient) AND variation (e.g. standard deviation) or associated estimates of uncertainty (e.g. confidence intervals)
- For null hypothesis testing, the test statistic (e.g. F , t , r) with confidence intervals, effect sizes, degrees of freedom and P value noted
Give P values as exact values whenever suitable.
- For Bayesian analysis, information on the choice of priors and Markov chain Monte Carlo settings
- For hierarchical and complex designs, identification of the appropriate level for tests and full reporting of outcomes
- Estimates of effect sizes (e.g. Cohen's d , Pearson's r), indicating how they were calculated
- Clearly defined error bars
State explicitly what error bars represent (e.g. SD, SE, CI)

Our web collection on [statistics for biologists](#) may be useful.

Software and code

Policy information about [availability of computer code](#)

Data collection

Data collection did not involve the use of software.

Data analysis

```
-R version 3.5.1 (2018-07-02)
-Platform: x86_64-apple-darwin15.6.0 (64-bit)
Running under: macOS 10.14- attached base packages:
stats, graphics, grDevices, utils, datasets, methods, base
- IMOD version 4.9.4
- other attached packages:
mcclust_1.0, lpSolve_5.6.13, NbClust_3.0, factoextra_1.0.5, bindrcpp_0.2.2, gridExtra_2.3, cluster_2.0.7-1, ggthemes_4.0.1,
forcats_0.3.0, stringr_1.3.1, dplyr_0.7.7, purrr_0.2.5, readr_1.1.1, tidyr_0.8.2, tibble_1.4.2, tidyverse_1.2.1, DT_0.5, caret_6.0-80,
ggplot2_3.1.0, lattice_0.20-35, rmarkdown_1.10, nvimcom_0.9-71
```

For manuscripts utilizing custom algorithms or software that are central to the research but not yet described in published literature, software must be made available to editors/reviewers upon request. We strongly encourage code deposition in a community repository (e.g. GitHub). See the Nature Research [guidelines for submitting code & software](#) for further information.

Data

Policy information about [availability of data](#)

All manuscripts must include a [data availability statement](#). This statement should provide the following information, where applicable:

- Accession codes, unique identifiers, or web links for publicly available datasets
- A list of figures that have associated raw data
- A description of any restrictions on data availability

Gene identifiers are provided within the manuscript. There are no restrictions of data availability.

Field-specific reporting

Please select the best fit for your research. If you are not sure, read the appropriate sections before making your selection.

Life sciences Behavioural & social sciences Ecological, evolutionary & environmental sciences

For a reference copy of the document with all sections, see [nature.com/authors/policies/ReportingSummary-flat.pdf](https://www.nature.com/authors/policies/ReportingSummary-flat.pdf)

Life sciences study design

All studies must disclose on these points even when the disclosure is negative.

Sample size	Micrographs are representative images obtained from at 3-4 independent biological samples, apart from TEM tomographs shown in Figures 2 and 4, which were obtained from two one representative biological sample, respectively. Each biological replicate consisted of a minimum of 5 root samples which were excised into 1-2mm pieces. Three to five root pieces were randomly selected for high pressure freezing (per planchette) and 3-5 planchettes pooled for freeze substitution and to generate blocks for TEM analysis. Two different freeze substitution (FS) methods were used, which generated similar results. Therefore each biological sample consisted of at least 9-25 root pieces for each FS round. A minimum of four blocks from each FS method were randomly selected from each biological replicate for sectioning and TEM imaging.
Data exclusions	no data were excluded
Replication	TEM tomographs shown in Figures 2 and 4 were taken from two and one representative biological samples, respectively, which were taken from blocks that were preselected based on the presence of EVs and fungal memtub structures. To ensure reproducibility of our experimental findings blocks for TEM analysis were selected randomly from pooled root samples and processed using two independent freeze substitution methods.
Randomization	Root tissue was collected from independent roots of independent plants from independent experiments. Apart from TEM tomography, blocks used for TEM analysis were selected randomly as described above.
Blinding	Microscopy-based study

Reporting for specific materials, systems and methods

Materials & experimental systems

n/a	Involved in the study
<input type="checkbox"/>	<input checked="" type="checkbox"/> Unique biological materials
<input checked="" type="checkbox"/>	<input type="checkbox"/> Antibodies
<input checked="" type="checkbox"/>	<input type="checkbox"/> Eukaryotic cell lines
<input checked="" type="checkbox"/>	<input type="checkbox"/> Palaeontology
<input checked="" type="checkbox"/>	<input type="checkbox"/> Animals and other organisms
<input checked="" type="checkbox"/>	<input type="checkbox"/> Human research participants

Methods

n/a	Involved in the study
<input checked="" type="checkbox"/>	<input type="checkbox"/> ChIP-seq
<input checked="" type="checkbox"/>	<input type="checkbox"/> Flow cytometry
<input checked="" type="checkbox"/>	<input type="checkbox"/> MRI-based neuroimaging

Unique biological materials

Policy information about [availability of materials](#)

Obtaining unique materials *Describe any restrictions on the availability of unique materials OR confirm that all unique materials used are readily available*

Obtaining unique materials *(from the authors or from standard commercial sources (and specify these sources)).*